



Pressure Oscillation Analysis in the Recoil Mechanism

Kunpeng Sun, Yadong Xu*

School of Mechanical Engineering, Nanjing University of Science and Technology, Nanjing 210094, China

*Corresponding author's e-mail: ydxu@njjust.edu.cn

Abstract. A periodic oscillation in the working chamber pressure was observed in the pressure test data of the recoil mechanism, with an amplitude accounting for 6% of the maximum pressure. This pressure fluctuation affects the calculation of the hydraulic resistance of the recoil mechanism. In previous studies, pressure oscillations were generally considered to be noise introduced by sensors, and earlier calculation methods failed to capture the pressure oscillations in the working chamber. Since the outer tube of the recoil mechanism is a thin-walled, long-cylinder component, this study takes its radial expansion stiffness into account and establishes an equivalent spring-mass model, using a non-oscillatory pressure curve as the model input. The comparison between the calculation results and experimental data shows that the calculated curves under different operating conditions closely match the experimental curves. Moreover, the oscillation frequency of the calculated results is very close to that of the experimental results, indirectly proving that the pressure oscillations in the working chamber of the recoil mechanism are caused by the radial expansion of the outer tube.

Keywords: Recoil mechanism; Thin-walled structure; Radial expansion stiffness; Pressure oscillation

1 Introduction

The recoil mechanism is an essential component of the artillery's firing system. It generates hydraulic resistance through the principle of throttling via small orifices, significantly reducing the impact loads during the firing process^[1]. Therefore, the calculation of the hydraulic resistance in the recoil mechanism is a key aspect of its structural design. The current hydraulic resistance calculation formula is based on the assumption of one-dimensional steady-state incompressibility, which results in significant calculation errors. Zheng Jianguo established a two-dimensional turbulent flow calculation model and obtained hydraulic resistance curves through numerical simulations, thereby improving the accuracy of hydraulic resistance calculations^[2]. Some scholars used dynamic mesh calculations in CFD software to accurately simulate the distribution of the internal flow field. This allowed for the acquisition of pressure data for each chamber of the recoil mechanism, making the flow field characteristics of the recoil mechanism

clearer^[3,4]. Miao Wei et al. used a hydraulic node model and considered the compressibility and phase change of the recoil fluid. The calculated pressures for each chamber were found to be very close to the experimental results^[5].

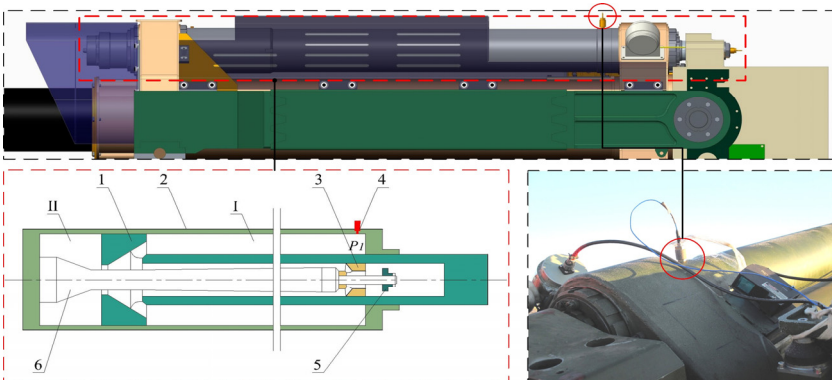
On the other hand, some scholars^[6,7] have used multi-objective optimization methods to optimize the structure of the throttling bar, reducing the peak hydraulic resistance and improving the buffering performance of the recoil mechanism. Other scholars^[8,9] have used intelligent algorithms to identify hydraulic resistance coefficients, thereby enhancing the accuracy of hydraulic calculations.

In current research on recoil mechanisms, scholars have focused on studying the internal flow field characteristics or resistance coefficients, which have contributed to making hydraulic resistance calculations closer to the actual values. However, no scholars have considered the impact of the thin-walled structure of the recoil mechanism on the pressure in each chamber. This study establishes a spring-mass dynamic model for the outer tube of the recoil mechanism and investigates the effect of the radial expansion stiffness of the outer tube on the pressure in the working chamber of the recoil mechanism.

2 Pressure Oscillation in the Working Chamber of the Recoil Mechanism

2.1 Experimental Process

This study takes a certain vehicle-mounted cannon firing test as an example. Pressure sensors were installed at the bottom of the recoil mechanism's outer tube, as shown in Figure 1, to measure the time-dependent pressure data of the working chamber during the recoil process. To minimize experimental variability, multiple firing angles and different charge numbers were tested. The experiment obtained multiple sets of valid working chamber pressure data for the recoil mechanism.



(1: piston rod; 2: outer tube; 3: counter-recoil throttling piston; 4: pressure sensor for P_I ; 5: valve; 6: throttling bar; I:working chamber; II:non-working chamber 2).

Fig. 1. The diagram of sensor installation locations

The pressure data from the working chamber under three different operating conditions are selected, as shown in Figure 2. In all three sets of experimental data, periodic oscillations are present throughout the pressure curves. Around 16ms, due to the closure of the crescent groove, the flow passage area decreases sharply, forcing a sudden change in flow, resulting in a significant pressure shock in the working chamber [5]. This shock causes the pressure oscillation pattern in the working chamber to be unclear before 40ms. After 40ms, the pressure shock effect gradually dissipates, and the overall pressure stabilizes, making the pressure oscillation pattern in the working chamber more distinct.

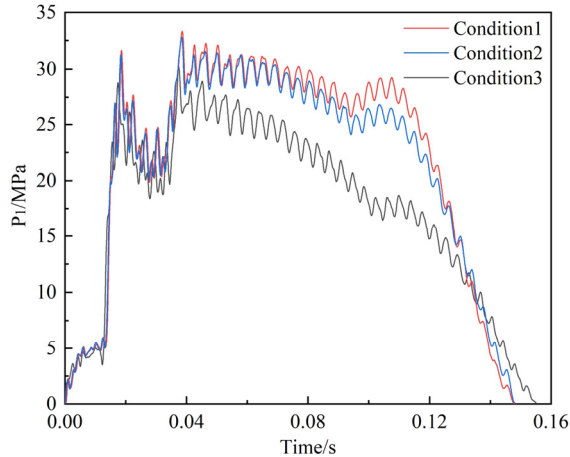


Fig. 2. P_1 under different working conditions.

In these three sets of experimental data, the pressure oscillation pattern after 40ms is clear, and there is no interference from pressure shocks. Therefore, the pressure data from this segment is taken as the subject of study. The oscillation periods of pressure in the three sets of data are essentially consistent.

2.2 Analysis of the Oscillation Causes

The working chamber of the recoil mechanism is composed of the outer tube and the recoil piston rod. The recoil rod moves with the artillery breech, and the hydraulic resistance is transmitted through the recoil rod to the recoil body, thereby cushioning the impact load during firing [10]. In the design criteria of the recoil mechanism, the wall thickness of the outer tube only needs to ensure safety under the working chamber pressure. To reduce the overall mass, the outer tube wall is relatively thin, and the outer tube is generally long. In such a thin-walled, long cylindrical structure, the radial elastic stiffness of the tube wall cannot be ignored [11]. In this case, the outer tube of the recoil mechanism exhibits radial expansion stiffness, and under the action of the working chamber pressure, it forms a spring-mass model, resulting in periodic oscillations in the working chamber pressure.

3 Establishment of the Calculation Model

3.1 Spring-Mass Model of the Recoil Mechanism Outer Tube

In the spring-mass model of the recoil mechanism's outer tube, it is assumed that the fluid in the working chamber is incompressible and only transmits pressure without participating in the oscillation. Thus, the outer tube of the recoil mechanism acts both as a mass (the oscillator) and a spring.

The spring stiffness in the hydraulic cylinder is a series combination of the radial expansion stiffness of the cylinder's outer tube, the elongation stiffness of the piston rod, and the compressibility of the fluid [12]. The structure of the recoil mechanism is similar to that of a hydraulic cylinder. However, since the recoil rod has a large diameter and a high elongation stiffness, and the compressibility of the fluid is neglected, the effects of the recoil rod's elongation stiffness and fluid compressibility are disregarded in this study. Therefore, the spring stiffness in the spring-mass model is taken as the radial expansion stiffness K_c of the recoil mechanism's outer tube.

$$K_c = \frac{E_c S_c}{2L_e \left(\frac{d_c^2 + D_c^2}{d_c^2 - D_c^2} + \nu_c \right)} \quad (1)$$

The material of the outer tube is 35Cr. The elastic modulus of the outer tube material, E_c , is 210 GPa; the working chamber area, S_c , is 0.0158 m²; the outer diameter of the outer tube, d_c , is 0.187 m; the inner diameter of the outer tube, D_c , is 0.168 m; the Poisson's ratio of the outer tube material, ν_c , is 0.3. The effective length of the outer tube, L_e , is considered constant during the recoil process, as there is no pressure acting on the non-working chamber fluid and the outer tube is fixed at both ends. Since the connection parts at both ends are relatively thick and their length is neglected, L_e is taken as 1.75 m, which is the length of the entire outer tube.

In the oscillation model constituted by the radial expansion stiffness of the recoil mechanism's outer tube, since the outer tube is fixed at both ends and free in the middle, and considering that the wall thickness of the outer tube is uniform along its effective length, the outer tube's expansion motion can be equivalently modeled as having half of the outer tube's mass participating in free vibration. Therefore, the mass of the oscillator, m , is taken as half of the mass of the thin-walled outer tube of the recoil mechanism.

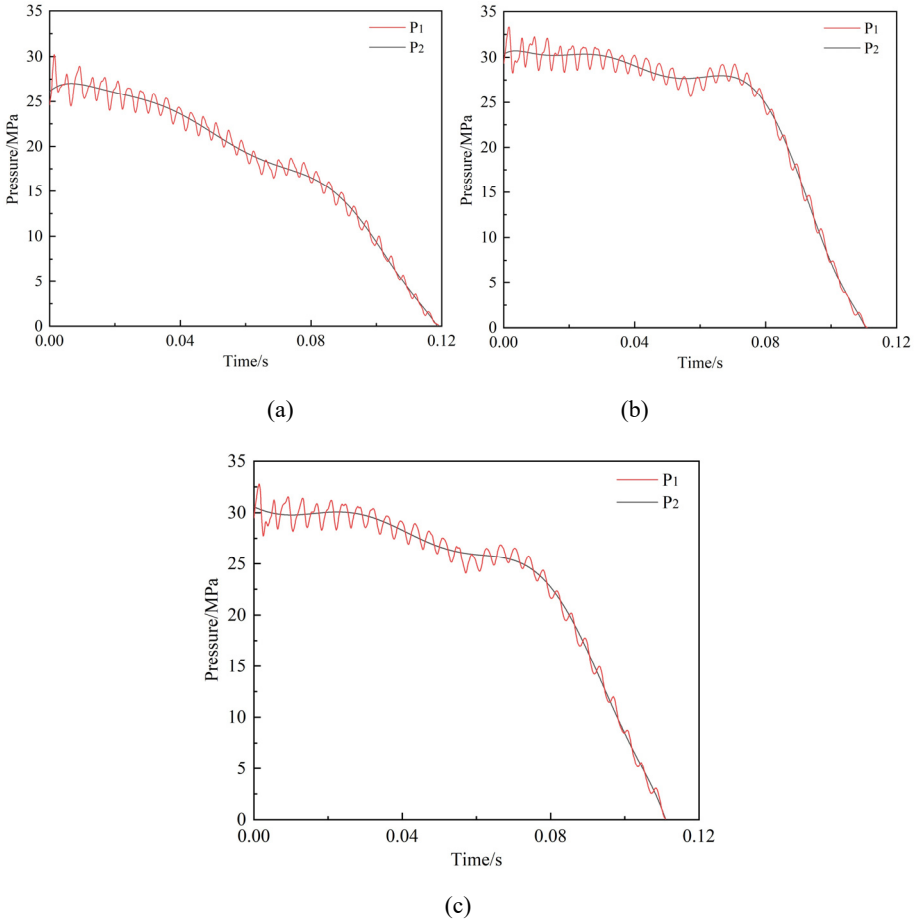
$$m = \frac{1}{2} \rho L_e (d_c^2 - D_c^2) \quad (2)$$

3.2 Input Load

The most obvious oscillation interval of the working chamber pressure P_l from three sets of recoil mechanism test data is selected as the subject of the study, as shown in

Figure 3. The non-oscillatory curve within this interval is taken as the load input for the spring-mass model. To obtain the non-oscillatory pressure curve P_2 , a ninth-order polynomial is used to fit P_1 , approximating and replacing P_2 . Thus, the input force F_1 for the spring-mass model is:

$$F_1 = P_2 S_c \tag{3}$$



(a) working condition 1; (b) working condition 2; (c) working condition 3.

Fig. 3. Comparison of P_1 and P_2 under different working conditions:

At time zero in the three sets of data, there is a difference between P_2 and P_1 . That is, in the actual recoil mechanism's outer tube, at this moment, the outer tube has already been compressed or stretched. In the spring-mass model, this means that the spring has an initial preload F_2 at the initial moment. The size of the preload F_2 is given by:

$$F_2 = P_1(t_0) S_c \tag{4}$$

4 Establishment of the Dynamic Model and Result Analysis

In the dynamic software, the spring-mass model is established where the oscillator is connected to the ground through a moving joint. A spring force is applied between the oscillator and the ground. The mass of the oscillator is set as m , and the spring stiffness is K_c , with a preload F_2 . The magnitude of the force acting on the oscillator is set as F_1 , as shown in Figure 4.

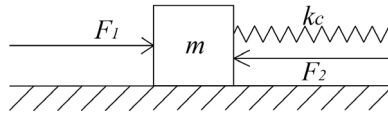
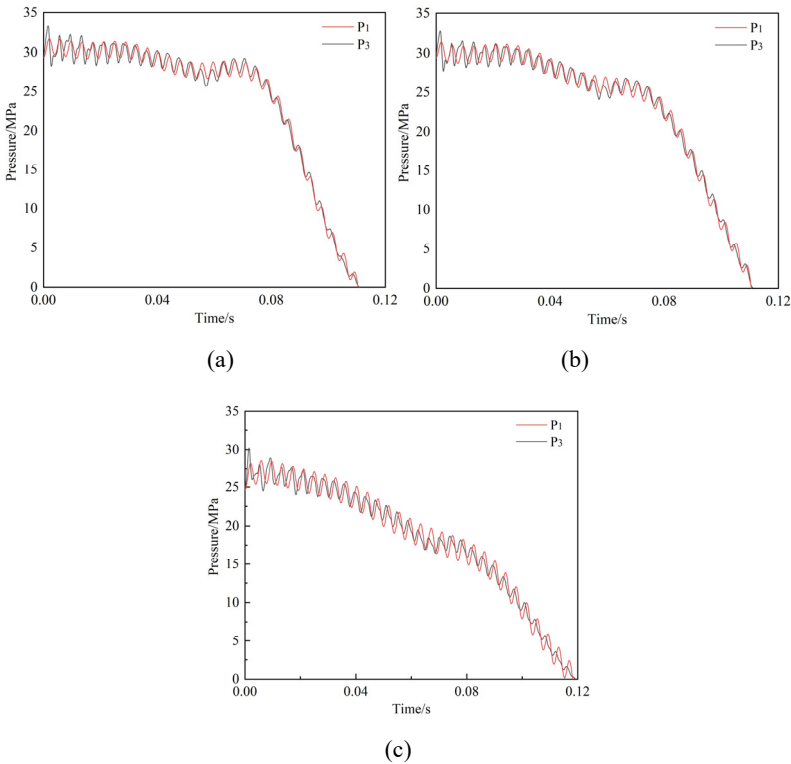


Fig. 4. Spring-mass model schematic.

The spring force in the simulation model is extracted and divided by the working chamber area to obtain the simulated working chamber pressure P_3 . The comparison between the simulation results and the experimental results is shown in Figure 5.



(a) working condition 1; (b) working condition 2; (c) working condition 3.

Fig. 5. Comparison of P_1 and P_3 under different working conditions:

Table 1. Comparison Between Experimental and Simulation Data.

Condition	Experimental oscillation period	Simulated oscillation period	Experimental number of peaks	Simulated number of peaks
1	3.828ms	3.825 ms	31	31
2	3.839ms	3.825 ms	29	29
3	3.839 ms	3.825 ms	29	29

As seen in the figure 5, the three sets of results show consistency. Taking the first set of results as an example, in the initial section of the curve, the oscillation amplitude of the experimental curve is larger than that of the simulation curve, and the experimental curve is not smooth. This is because the pressure shock effect caused by the closure of the crescent groove has not fully dissipated at this point. In the middle section of the curve, there is a deviation in amplitude between the fitted curve and the experimental curve, resulting in a larger offset between the simulation curve and the experimental curve in this region. As seen in the table 1, the oscillation frequency of the simulation closely matches the actual frequency, so throughout the entire curve, the number of peaks in the simulation curve matches the number of peaks in the experimental curve.

5 Conclusion

From the comparison between the calculation results and experimental data, it can be concluded that the spring-mass model of the recoil mechanism's outer tube established in this study matches the experimental data well. This indirectly suggests that the periodic oscillation of the working chamber pressure is caused by the expansion stiffness of the thin-walled structure of the recoil mechanism.

The oscillation amplitude of the working chamber pressure is 6% of the maximum pressure, which can lead to significant errors in the calculation of hydraulic resistance. Therefore, when designing the outer tube of the recoil mechanism, not only must the strength requirements be checked, but the stiffness should also be verified. This ensures that the working chamber pressure remains relatively stable.

Acknowledgments

This work was financially supported by the National Natural Science Foundation of China. (Grant Nos. U2341296)

References

1. GAO Shu-zi, CHEN Yun-sheng, ZHANG Yue-lin, et al. Gun recoil mechanism[M]. Beijing: Weapon Industry Press, 1995.
2. ZHENG J. Numerical Simulation of Flow Field in A Gun Recoil Mechanism [J]. Mechanics in Engineering, 2001, 23(2): 30-32.

3. Elsaady W A, Ibrahim A Z, Abdalla A A. Numerical simulation of flow field in coaxial tank gun recoil damper[J]. *Advances in Military Technology*, 2019, 14(1): 139-150.
4. Jevtić D, Micković D, Elek P, et al. Analysis of the influence parameters on the pressure field in the hydraulic mechanism[C]//9th International Scientific Conference–OTEH 2020, Belgrade, 8-9 October 2020. Belgrade: Military Technical Institute, 2020.
5. Miao W , Qian L , Chen L .Hydraulic node model and parameter identification of a dull recoil brake[J].*Journal of Mechanical Science and Technology*, 2022, 36(11):5511-5521.
6. Zhao J H. Optimal firing stability design for a gun[J]. *Journal of Vibration and Shock*, 2010, 29(11): 91-93.
7. ZONG S, QIAN L, XU Y. Dynamic coupling analysis and optimization of gun recoil mechanism[J]. *Acta Armamentarii*, 2007, 28(3): 272.
8. Bao D, Hou B. Parameters identification of a cannon counter-recoil mechanism based on PSO and interval analysis theory[J]. *Vibroengineering Procedia*, 2018, 20: 248-253.
9. GUO S. Simulation and parameters intelligent optimization of soft recoil system[C]//2020 Chinese Automation Congress (CAC). IEEE, 2020: 3663-3668.
10. Tan LB, Zhang XY, Pan XB, et al. *Introduction to Artillery*. Beijing: Beijing Institute of Technology Press; 2014.
11. Chen Zhiquan. *Coupling Dynamics and Reliability Optimization for Integrated Shell Luffing and Ramming Equipment of the Large Caliber Artillery* [D]. Nanjing University of Science and Technology, 2022.
12. Feng Hao. *Study on the flexible body dynamics and strength of excavator working device considering the characteristics of hydraulic cylinder* [D]. Guangzhou: South China University of Technology, 2018.

Open Access This chapter is licensed under the terms of the Creative Commons Attribution-NonCommercial 4.0 International License (<http://creativecommons.org/licenses/by-nc/4.0/>), which permits any noncommercial use, sharing, adaptation, distribution and reproduction in any medium or format, as long as you give appropriate credit to the original author(s) and the source, provide a link to the Creative Commons license and indicate if changes were made.

The images or other third party material in this chapter are included in the chapter's Creative Commons license, unless indicated otherwise in a credit line to the material. If material is not included in the chapter's Creative Commons license and your intended use is not permitted by statutory regulation or exceeds the permitted use, you will need to obtain permission directly from the copyright holder.

